Local Projections of Low-Momentum Potentials

K.A. Wendt* and R.J. Furnstahl† Department of Physics, The Ohio State University, Columbus, OH 43210

S. Ramanan[‡]

Department of Physics, Indian Institute of Technology, Chennai 600 036, India (Dated: November 4, 2018)

Nuclear interactions evolved via renormalization group methods to lower resolution become increasingly non-local (off-diagonal in coordinate space) as they are softened. This inhibits both the development of intuition about the interactions and their use with some methods for solving the quantum many-body problem. By applying "local projections", a softened interaction can be reduced to a local effective interaction plus a non-local residual interaction. At the two-body level, a local projection after similarity renormalization group (SRG) evolution manifests the elimination of short-range repulsive cores and the flow toward universal low-momentum interactions. The SRG residual interaction is found to be relatively weak at low energy, which motivates a perturbative treatment.

PACS numbers: 21.30.-x,05.10.Cc,13.75.Cs

I. INTRODUCTION

Nuclear two-body interactions found in textbooks are readily visualized because they are usually local; that is, they are radially diagonal in coordinate representation (e.g., see Refs. [1-3]). Plots of the central part of the potential, for example, exhibit long-range attraction from one-pion exchange, moderate mid-range attraction, and strong short-range repulsion. The long-range behavior is established from general considerations of spontaneously broken chiral symmetry [4] but the short-range features are tied to the constraint of locality. That is, a repulsive core is the inevitable consequence of fitting a local nucleon-nucleon (NN) interaction to S-wave scattering phase shifts beyond energies where they turn repulsive. While short-range locality is not a physical requirement [5], the associated short-range correlations (SRC) induced by the repulsive core provide intuition for nuclear observables, such as those associated with highmomentum-transfer probes [6].

Local potentials are an advantage or even a necessity for some methods of solving the nuclear many-body problem. In particular, current implementations of quantum Monte Carlo, such as Green's function Monte Carlo (GFMC) [7, 8] and auxiliary field diffusion Monte Carlo (AFDMC) [9] require interactions that are expressed in an operator basis multiplying local functions of internucleon distances (e.g., Argonne v_{18} [10]). On the other hand, the repulsive core makes such potentials ill-suited for basis expansions used in configuration interaction (CI) and coupled cluster (CC) methods because the basis sizes required for convergence grow too large. Instead one turns to softened nuclear potentials, which sup-

press coupling between low- and high-momentum components and thereby exhibit greatly improved convergence. Examples of soft NN potentials include chiral effective field theory potentials with cutoffs of order 500 to 600 MeV [4, 11, 12] and renormalization group (RG) evolved interactions [13].

These low-momentum interactions are naturally developed and visualized in momentum representation, where the coupling of momentum scales can be interpreted via scattering theory [13]. However, softening from the RG is accompanied by induced non-locality, which obfuscates the nature of the softening in coordinate representation. Indeed their features in coordinate space have only been inferred rather than directly visualized. This has left open questions about the nature and consequences of the non-locality. For example, the elimination of short-range correlations with softening has been associated with the elimination of the repulsive core, but only by implication. Can it be directly visualized and how does this change SRC intuition? Is the long-range part unchanged? How is the RG flow toward universal low-momentum interactions manifested in coordinate representation? Is there a way to use the non-local low-momentum interactions with modern QMC techniques?

To address these questions, in this paper we explore a simple "local projection" for two-body potentials that separates softened non-local interactions into a local effective interaction plus a non-local residual interaction in each partial wave. This provides a natural visualization of the range-dependent features as the potential is evolved by RG methods. There is no unique projection at short distances, which gives us wide freedom to choose a form for the projection that reduces to local pion exchange at large separations ($r\gg 1$ fm). In Section II, we present a particular projection and describe its application and properties. Projections are made of evolved similarity renormalization group (SRG) potentials [13] starting from Argonne v_{18} [10] and from the Entem-Machleidt

^{*} wendt.31@osu.edu

[†] furnstahl.1@osu.edu

[‡] suna@physics.iitm.ac.in

500-MeV-cutoff chiral EFT potential [11] are given in Section III. The resulting local potentials demonstrate the elimination of short-range repulsive cores and the flow toward universal low-momentum interactions. In Section IV, the SRG residual interaction is shown to be relatively weak and we test its inclusion in perturbation theory. We summarize and outline further implications and applications in Section V.

II. BACKGROUND

We consider functionals that take a two-body potential that is dependent on both coordinate indices and produce a local interaction multiplying a delta function:

$$L[V(\mathbf{r}, \mathbf{r}')] = \delta(\mathbf{r} - \mathbf{r}') f(\mathbf{r}) . \tag{1}$$

We call L a local projection if it acts as an identity functional for already local potentials,

$$L[L[V(\mathbf{r}, \mathbf{r}')]] = L[V(\mathbf{r}, \mathbf{r}')]. \qquad (2)$$

Our original motivation was simply to visualize what is happening at different length scales in coordinate representation as the SRG (or another transformation) is applied to soften two-nucleon (and three-nucleon) interactions. However, such projections can also be used to decouple local and purely non-local components of the interaction for calculations.

Perhaps the simplest possible choice for a local projection is

$$L[V(\mathbf{r}, \mathbf{r}')] = \delta(\mathbf{r} - \mathbf{r}') \int d\mathbf{r}'' \ V(\mathbf{r}, \mathbf{r}'')$$
$$\equiv \delta(\mathbf{r} - \mathbf{r}') \overline{V}(\mathbf{r}) \ , \tag{3}$$

which sums at each ${\bf r}$ the interaction weight from the connected ${\bf r}''$ coordinates, essentially averaging over the non-locality. This should capture most of the effect of the potential on long-wavelength nucleons. It is clear that this functional acts as the identity for local potentials. That is, if $V({\bf r},{\bf r}')=V({\bf r})\delta({\bf r}-{\bf r}')$, then

$$\overline{V}(\mathbf{r}) = \int d\mathbf{r}'' V(\mathbf{r}) \delta(\mathbf{r} - \mathbf{r}'') = V(\mathbf{r}) . \tag{4}$$

Here and for the remaining discussion we drop the common factor $\delta(\mathbf{r} - \mathbf{r}')$ from the definition and work only with the function $\overline{V}(\mathbf{r})$ multiplying it.

This instance of local projection is not useful for tensor forces or terms local in only the radial coordinate, such as spin-orbit terms of the form $f(r)\mathbf{L}\cdot\mathbf{S}$. To deal with such terms, we extend the definition to apply in a coupled partial wave basis. A natural extension is:

$$\overline{V}_{l'm'}^{lm}(r) = \int d\Omega_{\mathbf{r}} \int_{0}^{\infty} d\mathbf{r}' Y_{lm}^{*}(\Omega_{\mathbf{r}}) Y_{l'm'}(\Omega_{\mathbf{r}'}) V(\mathbf{r}, \mathbf{r}')$$

$$= \int_{0}^{\infty} r'^{2} dr' V_{l'm'}^{lm}(r, r') . \tag{5}$$

This leaves unchanged local operators such as those in the Argonne v_{18} interaction, where

$$V_{l'm'}^{lm}(r,r') = V_{l'm'}^{lm}(r) \frac{\delta(r-r')}{r'^2} . \tag{6}$$

We define our partial wave expansion to have unit normalization,

$$V(\mathbf{r}, \mathbf{r}') = \sum_{lm} \sum_{l'm'} Y_{lm}^*(\mathbf{r}) Y_{l'm'}(\mathbf{r}') V_{l'm'}^{lm}(r, r') , \quad (7)$$

and to be symmetric between momentum and coordinate representations,

$$V(\mathbf{k}, \mathbf{k}') = \sum_{lm} \sum_{l'm'} Y_{lm}^*(\mathbf{k}) Y_{l'm'}(\mathbf{k}') V_{l'm'}^{lm}(k, k') . \quad (8)$$

Two-nucleon SRG interactions are usually computed directly in momentum representation [13] and it is therefore convenient to express the projection Eq. (5) in that basis. This follows by inserting the Fourier transform of the momentum-space interaction and calculating the free coordinate integral analytically, yielding

$$\overline{V}_{00}^{lm}(r) = \int_{0}^{\infty} k^{2} dk \ j_{l}(kr) V_{00}^{lm}(k,0)$$
 (9)

and (for l, l' > 0)

$$\overline{V}_{l'm'}^{lm}(r) = N_{ll'} \int_0^\infty dk dk' \, \frac{k^2}{k'} j_l(kr) V_{l'm'}^{lm}(k,k') \,, \quad (10)$$

where

$$N_{ll'} = \frac{4}{\sqrt{\pi}} \frac{\Gamma(\frac{l'+3}{2})}{\Gamma(l'/2)} i^{l'-l} . \tag{11}$$

This projection provides a useful starting point for visualizing what is happening at long and short distances as we make an RG evolution of the interaction. However, it is not unique and we have no evidence that it is an optimal separation of a local part of the interaction for calculations. From this point forward, we will only consider potentials that are rotationally invariant, so that the m, m' dependence is a Kronecker delta function, which will be suppressed.

To compare the relative strength of the local projection to the remaining non-local residual interaction $(V - \overline{V})$, we will use the Fourier transform of the local projection,

$$\overline{V}_{l'm'}^{lm}(k,k') = \frac{2}{\pi} \int_0^\infty r^2 dr j_l(kr) j_{l'}(k'r) \overline{V}_{l'm'}^{lm}(r) . \quad (12)$$

Expressing this momentum-space local projection directly in terms of the original momentum-space non-local potential is helpful to understand how universal features of SRG-evolved interactions affect the projection and how non-local features affect expectation values. For even l and l', a direct expression is known:

$$\overline{V}_{l'm'}^{lm}(k,k') = \frac{2}{\pi} \int_0^\infty q^2 dq \ I(l,l,l' \ q,k,k') f_{l'm'}^{lm}(q) \ , \quad (13)$$

where

$$f_{l'm'}^{lm}(q) = \begin{cases} V_{00}^{lm} V_{l0}(q,0) & \text{if } l' = 0, \\ V_{l'm'}^{00}(q,0) & \text{if } l = 0, \\ N_{ll'} \int dq' \ {q'}^{-1} V_{l'm'}^{lm}(q,q') & \text{otherwise,} \end{cases}$$
(14)

and I(l, l, l' q, k, k') is an integral of three spherical Bessel functions given in Ref. [14]. It is also numerically more stable to evaluate Eq. (13) instead of Eq. (12). For the figures presented here, we need:

$$I(0,0,0,q,k,k') = \frac{\pi \triangle (q,k,k')}{4qkk'}, \qquad (15)$$

$$I(0,0,2,q,k,k') = \frac{\pi \triangle (q,k,k')}{8qkk'^3} (k'^2 - 3(k-q)^2), \quad (16)$$

$$I(2,2,2,q,k,k') = -\frac{\pi \triangle (q,k,k')}{8qkk'^3} (3a^6 - 3Aa^4)$$

$$I(2, 2, 2 q, k, k') = -\frac{\pi \triangle (q, k, k')}{64q^3k^3k'^3} (3q^6 - 3Aq^4 - (2A^2 + B^2)q^2 + 3AB^2), \quad (17)$$

where $A \equiv k^2 + {k'}^2$, $B \equiv k^2 - {k'}^2$, and

$$\triangle(q, k, k') = \begin{cases} 1 & |k - k'| < q < k + k', \\ \frac{1}{2} & |k - k'| = q \text{ or } q = k + k', \\ 0 & \text{otherwise.} \end{cases}$$
 (18)

The expressions in Eqs. (13)–(18) provide insight by showing the different weightings of momentum regions for the S- and D-waves, as seen below.

III. VISUALIZATION

In this section, we use the local projection from Section II to construct simple visualizations of SRG-softened interactions [15, 16]. The SRG generates a continuous series of unitary transformations labeled by a parameter s,

$$H(s) = U(s)H(s=0)U^{\dagger}(s)$$
, (19)

which can be implemented as a flow equation [16, 17]

$$\frac{d}{ds}H(s) = \left[\eta(s), H(s)\right],\tag{20}$$

$$\eta(s) = \frac{dU(s)}{ds}U^{\dagger}(s) . \tag{21}$$

In the present studies, we use only the most common choice of $\eta(s)$ for nuclear applications,

$$\eta(s) = [T_{\text{rel}}, H(s)], \qquad (22)$$

which has demonstrated momentum decoupling properties [13, 18–26]. We use the momentum decoupling scale $\lambda = s^{1/4}$ (in units where $\hbar = c = m = 1$ with nucleon mass m) to label the evolution. In typical applications, λ ranges from ∞ (which is unevolved) to final values from 1.5 to $2.0\,\mathrm{fm}^{-1}$ [13].

In Figs. 1 to 4, the local projections from Section II are applied to the original and SRG-evolved Argonne v_{18} [10]

and Entem-Machleidt N³LO (500 MeV) [11] NN potentials in selected channels. These interactions are evolved in momentum representation from $\lambda = \infty$ (initial) to $\lambda = 1.6 \, \mathrm{fm}^{-1}$ and the local projection is calculated from the momentum representation. In each series of plots, the initial projected potentials are maintained as dashed lines for comparison to the evolved version and the region between the evolved projections is shaded to highlight the approach (or non-approach) to universal form.

The $\lambda = \infty$ panel in each of these figures shows the original Argonne v_{18} potential (up to small numerical artifacts from the use of finite momentum meshes) because it is local and projects onto itself. The effects of the strong short-range core are evident in all channels, with the peaks in the S-waves being off scale at over 2 GeV. The projection of the unevolved N³LO potential (which is not local) exhibits an overall oscillation with wavelength of about 2.5 fm, as would be expected from a momentum cutoff of 500 MeV. This cutoff is much lower than for Argonne v_{18} and therefore the potential is much softer, as shown by much weaker short-range contributions, which peak in the S-waves at about 140 MeV for the singlet channel and 200 MeV for the triplet channel. In the coupled ${}^{3}S_{1}-{}^{3}D_{1}$ channel in Fig. 1b, which includes contributions from the tensor force, we again see very strong effects at short distances for Argonne v_{18} and only relatively weak effects from the N³LO potential.

In the S-wave channels for Argonne v_{18} , Figs. 1a and 2 show that the SRG significantly modifies short-range features first as λ decreases, unlike in momentum representation where the initial modification occurs at all momenta. This is consistent with the modification taking the form of a regulated delta function in coordinate space, which is primarily a uniform shift in momentum space below the cutoff scale. Such a shift has been previously identified for the SRG [27, 28] and for the $V_{\text{low }k}$ RG [29]. We see a rapid and dramatic dissolution of the repulsive core and a relatively weak modification at longer ranges $(r > 2 \,\text{fm})$ once we have evolved below about $2 \,\text{fm}^{-1}$. That is, the core is largely removed before significant modification to the tail begins.

This "core meltdown" is qualitatively consistent with previous intuition about SRG evolution, but to our knowledge this is the first quantification of the size of the modification at both short and long ranges. The N³LO evolution is less dramatic, but equally complete in the suppression of short-range repulsion. Both projected potentials are completely attractive by $\lambda = 2 \, \text{fm}^{-1}$, except for small long-range oscillations. This is consistent with observed perturbative behavior in infinite nuclear matter, where the repulsion driving saturation originates with three-body forces [21, 30]. From this point on in the flow the potentials become increasingly alike at all distance scales, reflecting the flow toward universal form previously observed in momentum representation [13]. Because the local projection samples low-momentum matrix elements with greater weight than those at high momentum (see Eqs. (13)–(18)), low-momentum universal-

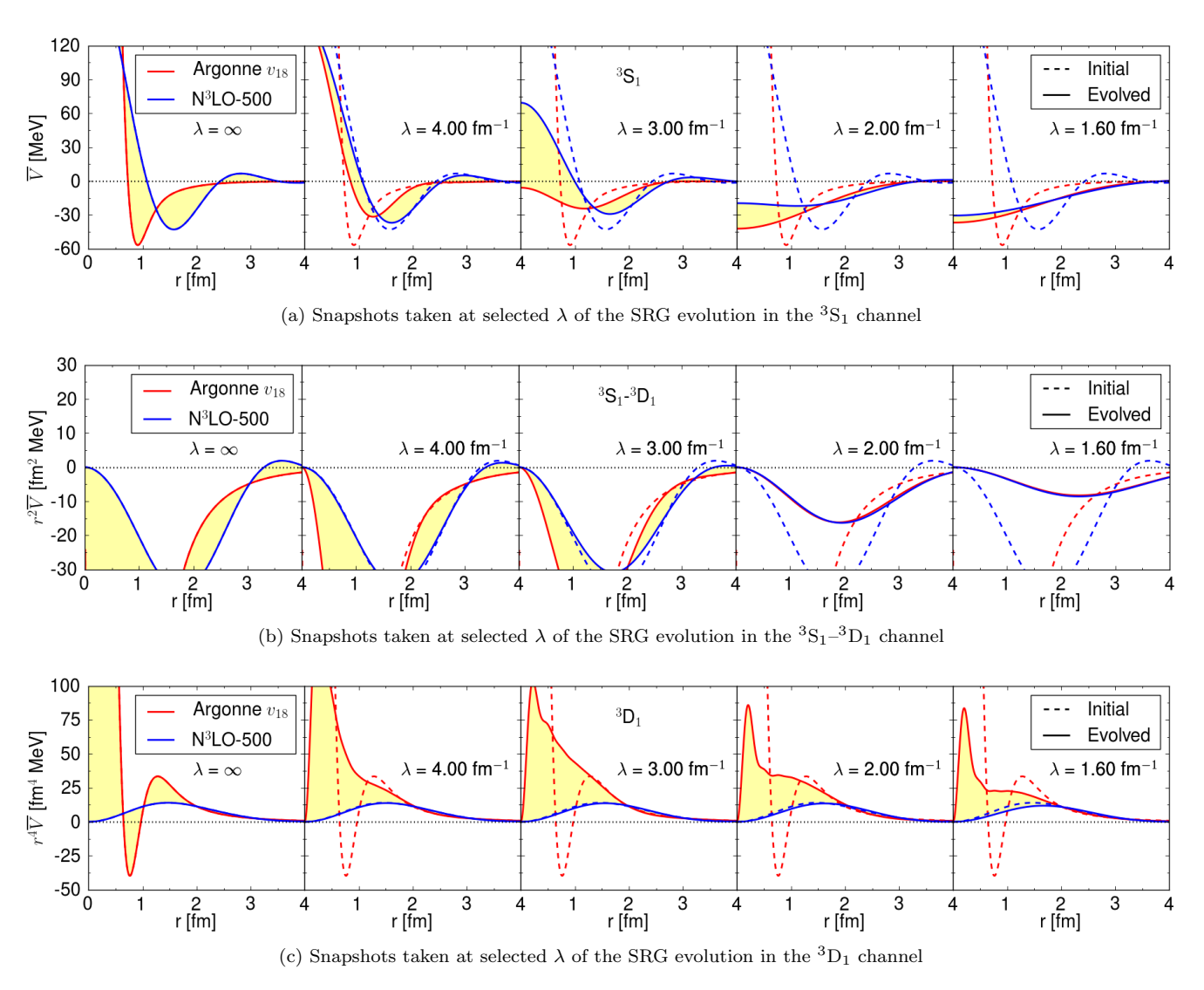


FIG. 1. (color online) SRG evolution of local projections for the deuteron NN channels, with the unevolved ($\lambda = \infty$) projected Argonne v_{18} [10] and N³LO (500 MeV) [11] potentials shown as dashed lines. The region between the potentials is shaded to highlight the approach to a universal form in the 3S_1 and 3S_1 – 3D_1 channels. The initial Argonne v_{18} potential is local and therefore its unevolved local projection is unchanged by local projection.

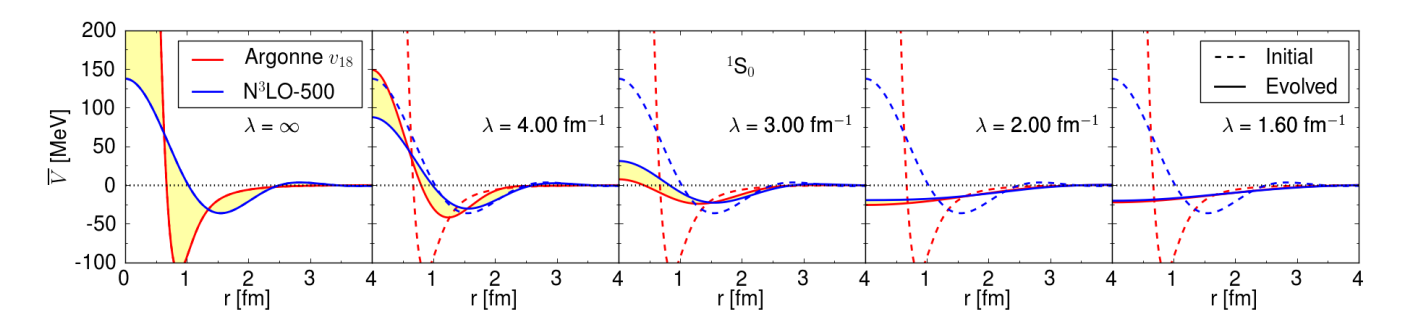


FIG. 2. (color online) SRG evolution of the local projections for the ${}^{1}S_{0}$ channel as in Fig. 1.

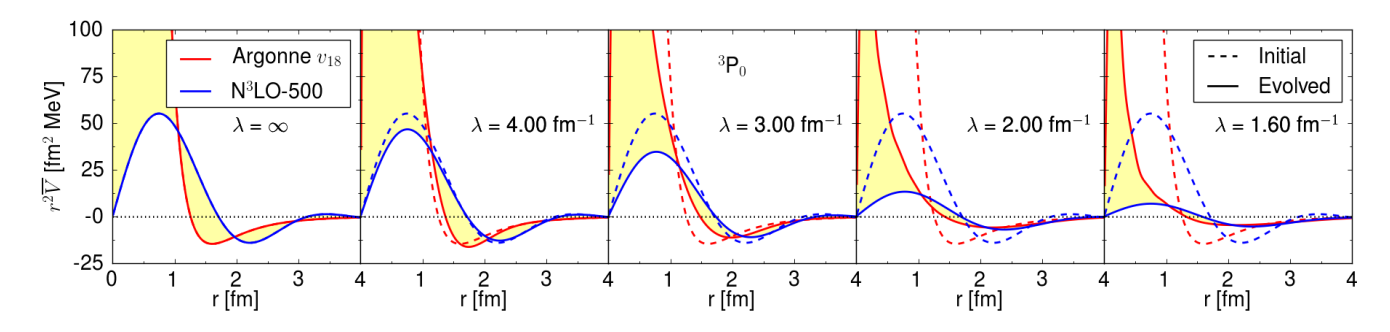


FIG. 3. (color online) SRG evolution of the local projections for the ³P₀ channel as in Fig. 1.

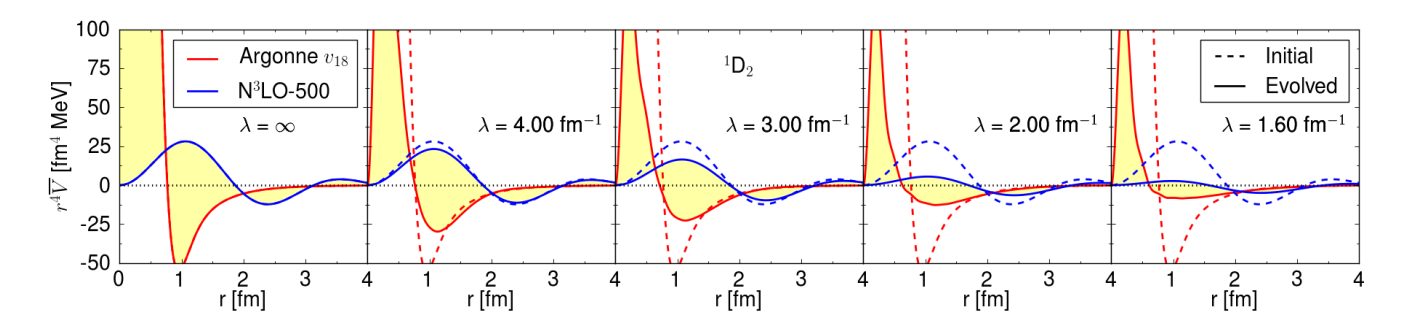


FIG. 4. (color online) SRG evolution of the local projections for the ¹D₂ channel as in Fig. 1.

ity translates to universality at all ranges in coordinate space for S-waves.

In the ${}^{3}S_{1}$ – ${}^{3}D_{1}$ coupled channel where the tensor force is active (see Fig. 1b), we observe dramatic reduction of short-range strength as a result of the SRG evolution. The initial N³LO projection already is weak compared to Argonne v_{18} , which is consistent with both the central suppression seen in the S-waves and the suppression of the tensor contribution by the 500 MeV cutoff. A universal form at all distance scales is seen already by $\lambda = 2 \, \text{fm}^{-1}$. In contrast, the projected potentials in the $^3\mathrm{D}_1$ channel in Fig. 1c are only equal for $r \geq 2\,\mathrm{fm}^{-1}$ and this is true for all λ . This contrasts with the Swave universality, largely because of the stronger weighting of high-momentum matrix elements in the local projection. The SRG evolution shows little modification of the N³LO potential at all λ while there is significant but incomplete (compared to the N³LO flow) modification of the Argonne v_{18} hard core.

The evolution in the ${}^{3}P_{0}$ channel (see Fig. 3) is qualitatively the same as the S-waves: strong reduction initially of short-range strength and later long-range modifications. However, it is less complete by the lowest λ and the results are less universal at short range. The same is true but to a greater extent in the ${}^{1}D_{2}$ channel (see Fig. 4). The reduced universality in the local projection is again a result of the stronger weighting of higher momenta when compared to the S-wave (see Eq. (13)). This results in the local projection matrix elements depending on diagonal matrix elements of the full interaction in the D-wave, peaking around $k = k' = \lambda$, where universal-

ity is incomplete. Note, however, that the effects of the residual short-range differences in matrix elements will be suppressed by the angular momentum barrier.

By taking the Fourier transform of a local projection and subtracting it from the original momentum-space potential, we can examine the residual non-local component of the interaction. This is shown for the $^1\mathrm{S}_0$ channel in Fig. 5 for Argonne v_{18} and in Fig. 6 for $\mathrm{N}^3\mathrm{LO}$. The $\lambda=\infty$ plots for $V-\overline{V}$ show the effect of the local projection on the initial potential: Argonne v_{18} is purely local and therefore $V-\overline{V}$ is identically zero, while the non-locality of $\mathrm{N}^3\mathrm{LO}$ is evident for $k,k'>2\,\mathrm{fm}^{-1}$. The dominant source of this non-locality is the ultraviolet regulator used, which is of the form f(k)f(k') where $f(k)\equiv e^{-(k^2/\Lambda^2)^n}$ with integer n and cutoff Λ . This is confirmed by observing the decrease in the non-local residual as Λ is increased.

We note that N^3LO is effectively local when at least one of k or k' is less than $1\,\mathrm{fm}^{-1}$. For both potentials, this region stays almost completely local during the full SRG evolution. Furthermore, the non-local component is relatively small elsewhere except near the large-momentum diagonal, which is decoupled from the low-energy physics. This suggests that the local projections can be more than a tool to visualize SRG evolved interactions, i.e., we may be able to treat SRG potentials as being local plus a small non-local part that can be handled in perturbation theory.

In summary, the local projections show that the potentials are modified by the SRG from the inside out (i.e., short-range first) as the decoupling scale λ is lowered.

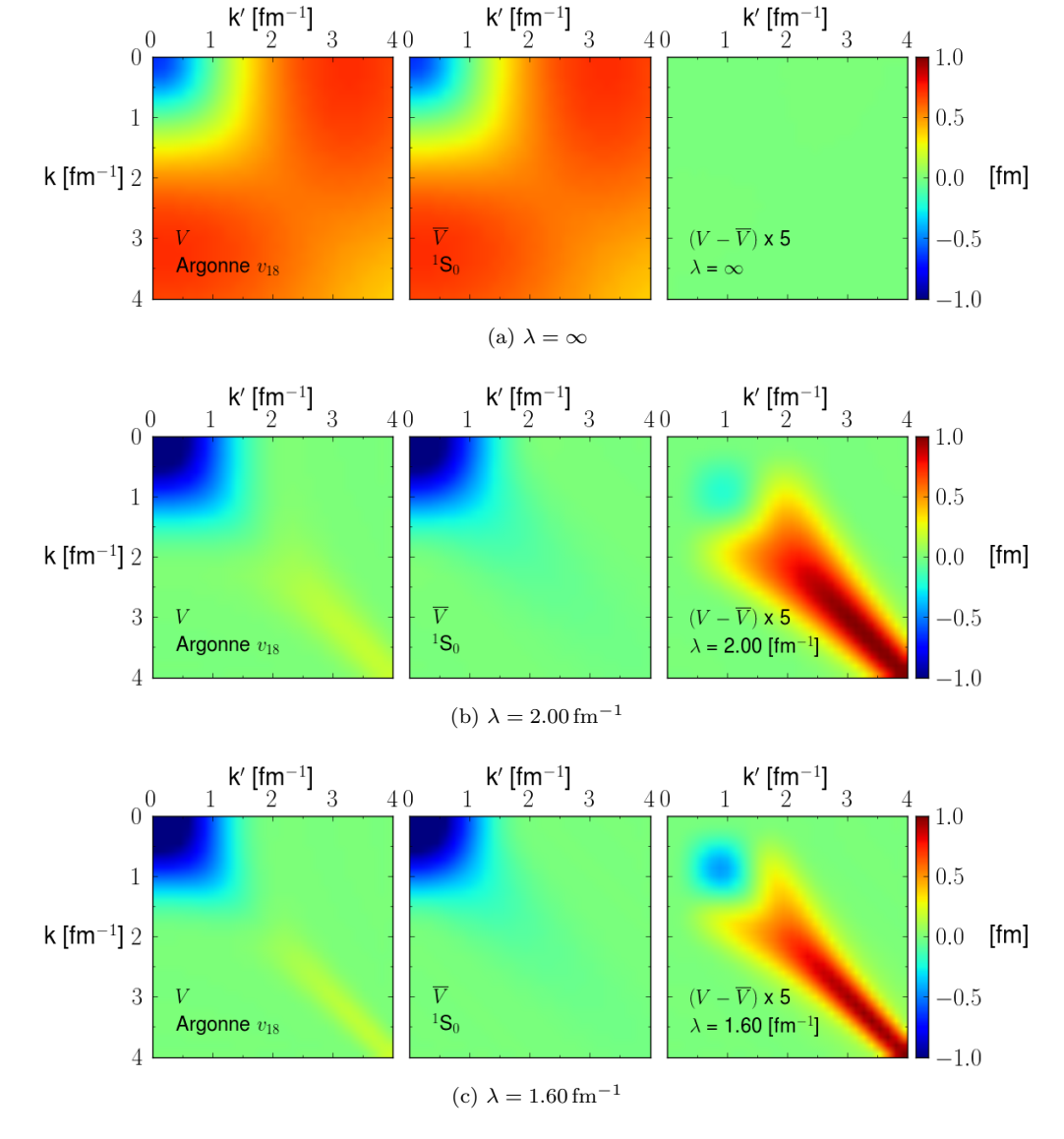


FIG. 5. (color online) Contour plots showing SRG evolution of the interaction (V), its local projection (\overline{V}) , and the residual non-local interaction $(V - \overline{V})$ multiplied by 5, starting from the Argonne v_{18} potential [10]. The initial potential $(\lambda = \infty)$ is local, as verified in (a), while the SRG evolution generates increasing non-locality.

The flow to universal form is cleanly seen in the S-waves, which become shallow and structureless attractive potentials. In the higher partial waves, a nearly universal form is reached except at the shortest ranges where the impact of the remaining discrepancies in matrix elements may be limited. Plots of the non-local residual interaction imply it is relatively weak in the low-momentum region, suggesting the applicability of perturbation theory, which we consider in the next section.

IV. PERTURBATION THEORY

In addition to providing a visualization of non-local NN forces, the local projection gives a well-defined non-local

residual interaction, $V - \overline{V}$. This residual by construction has no further local piece that can be extracted with the local projection used to compute \overline{V} :

$$L[V - \overline{V}] = L[V] - \overline{V} = \overline{V} - \overline{V} = 0.$$
 (23)

As we saw from Figs. 5 and 6, the low-momentum part of $\overline{V}(k,k')$ (i.e., for $k,k'\lesssim 1\,\mathrm{fm}^{-1}$) is almost completely local even after significant SRG evolution ($\lambda\lesssim 2\,\mathrm{fm}^{-1}$). This suggests that much of the low-energy physics is contained in the local interaction. Now we can ask how quantitatively we can reproduce low-energy observables using the local piece exactly with perturbative corrections from the non-local piece.

We start by considering phase shifts, using the distorted wave born approximation (DWBA) [31] to expand

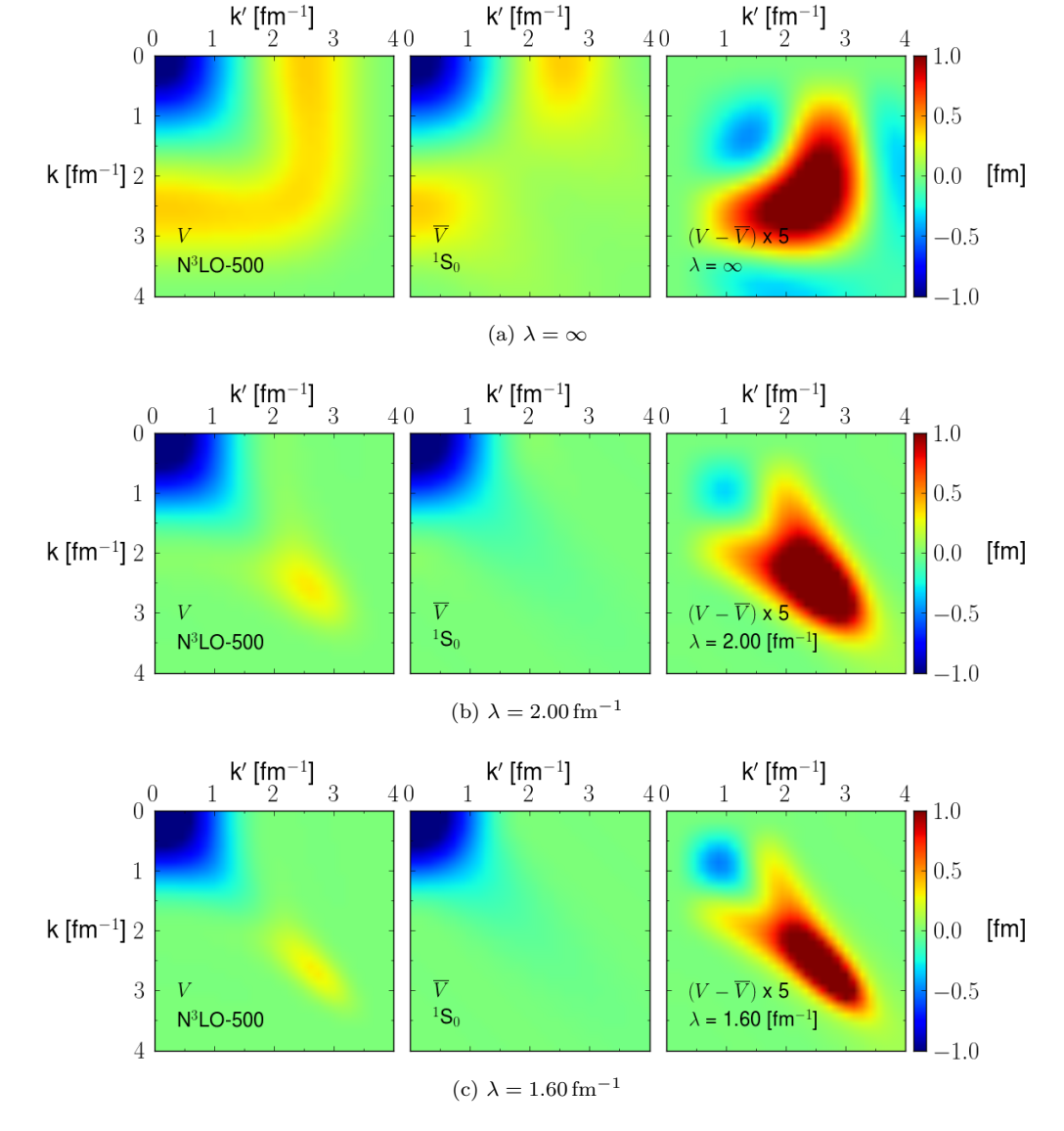


FIG. 6. (color online) Contour plots showing SRG evolution of the interaction (V), its local projection (\overline{V}) , and the residual non-local interaction $(V - \overline{V})$ multiplied by 5, starting from the N³LO potential of Ref. [11]. Even though the initial interaction is generally non-local, it is a nearly local potential at very low momentum.

about the local projection. Because we are working with the non-local residual interaction, the entire calculation is most convenient in momentum space. To proceed, we first compute the full momentum-space scattering wavefunction for the local projection in a single partial wave (we suppress dependence on l):

$$\langle k|\psi_p^+\rangle = \frac{A_p}{pk} \left[\delta(p-k) + B_p \mathcal{P} \frac{1}{p-k} + w_p(k)\right],$$
 (24)

where $B_p = -\pi^{-1} \tan(\delta_l(p))$ is real, $A_p = (1 + i\pi B_p)^{-1}$ is a complex coefficient, and $w_p(k)$ is a real regular function. These ingredients are computed non-perturbatively using the method described in Ref. [32]. We apply the two-potential formula [31, 33] to expand the exact half-on-shell partial-wave T-matrix in terms of the local scat-

tering function, keeping only the first-order correction:

$$T(k,k') = \langle k|\overline{V}|\psi_{k'}^{+}\rangle + \langle \psi_{k}^{-}|(V-\overline{V})|\chi_{k'}^{+}\rangle$$
$$\approx \langle k|\overline{V}|\psi_{k'}^{+}\rangle + \langle \psi_{k}^{-}|(V-\overline{V})|\psi_{k'}^{+}\rangle, \quad (25)$$

where $|\chi_k^+\rangle$ is the scattering wave function for the full potential and $|\psi_k^+\rangle$ is the scattering function for the local projected potential. We show representative results in Figs. 7 through 10 comparing phase shifts in the $^1\mathrm{S}_0$ and $^1\mathrm{D}_2$ partial waves calculated from the full potential, the local projection, and the first-order DWBA-corrected local projection at several stages in an SRG evolution.

Consider first the 1S_0 phase shifts in Figs. 7 and 8. The Argonne v_{18} potential is local, so for $\lambda = \infty$ the phase shifts from the projected potential are exact. In contrast, the phase shifts from the non-local unevolved

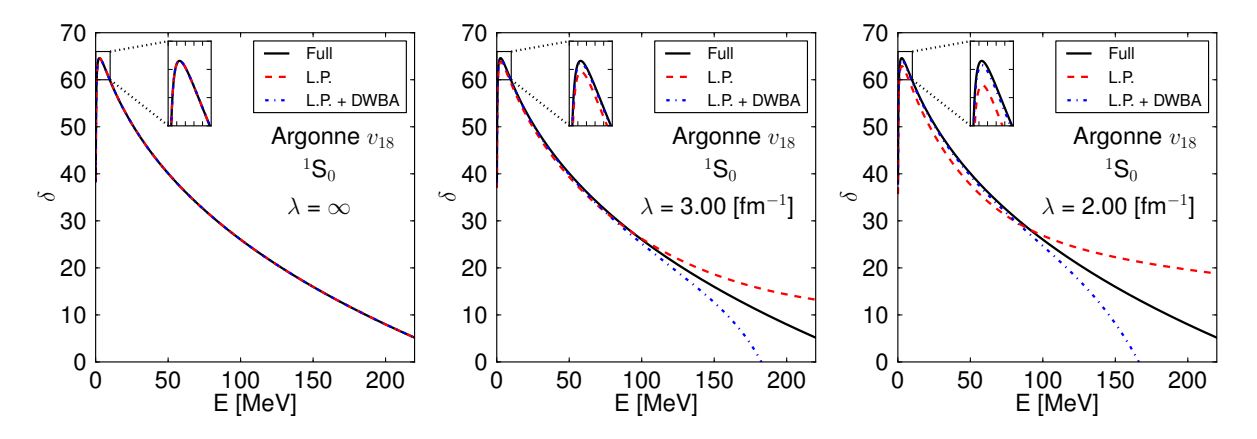


FIG. 7. (color online) Nucleon-nucleon phase shifts in the 1 S₀ channel at three stages of an SRG evolution ($\lambda = \infty$, 3 fm⁻¹, and 2 fm⁻¹) starting from Argonne v_{18} as the initial potential. In each panel, the phase shifts computed from the on-shell T-matrix for the full interaction (solid) are compared to those from the local projection alone (dashed) and from the projection plus a first-order DWBA correction (dotted). The insets show an expanded view at low energy.

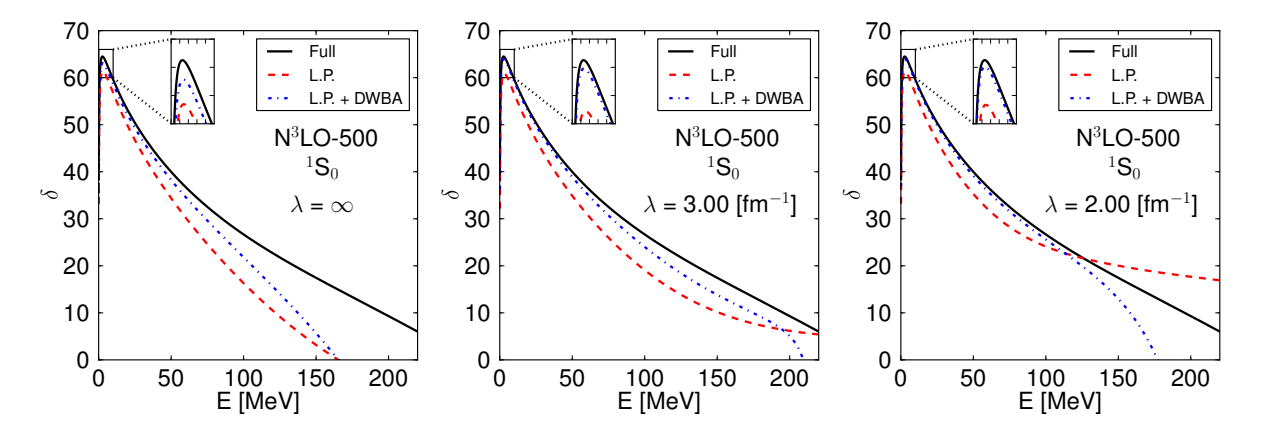


FIG. 8. (color online) Same as Fig. 7 except starting from Entem-Machleidt N³LO 500 MeV as the initial potential.

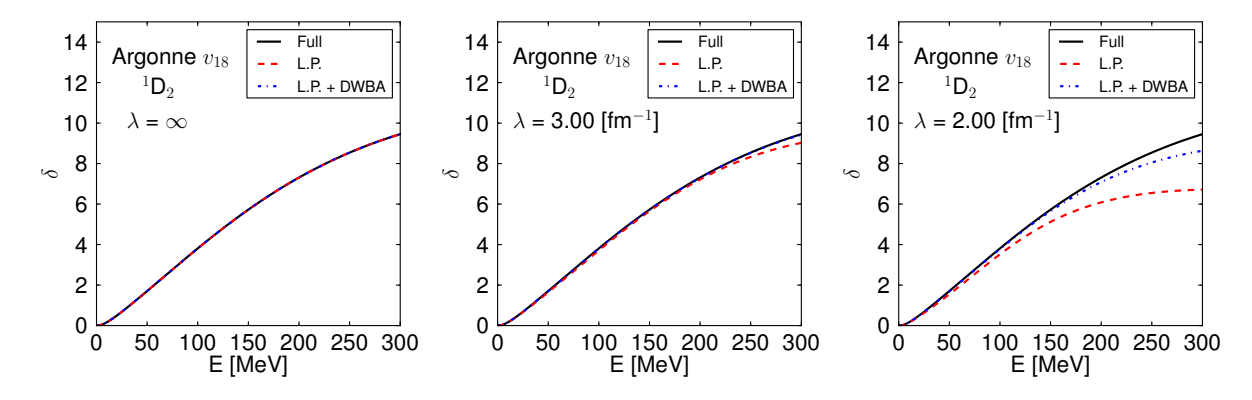


FIG. 9. (color online) Nucleon-nucleon phase shifts in the $^{1}D_{2}$ channel at three stages of an SRG evolution ($\lambda = \infty$, 3 fm^{-1} , and 2 fm^{-1}) starting from Argonne v_{18} as the initial potential. In each panel, the phase shifts computed from the on-shell T-matrix for the full interaction (solid) are compared to those from the local projection alone (dashed) and from the projection plus a first-order DWBA correction (dotted). The insets show an expanded view at low energy.

 $\rm N^3LO$ potential are modified by the projection at all energies. The first-order perturbative correction improves the agreement everywhere, but there remains significant disagreement above 100 MeV. As the Argonne v_{18} potential

is evolved, the local projection increasingly deviates from the exact phase shifts below $100\,\mathrm{MeV}$, but the first-order correction restores agreement to the one percent level. We note that reconstructing the low-energy peak in this

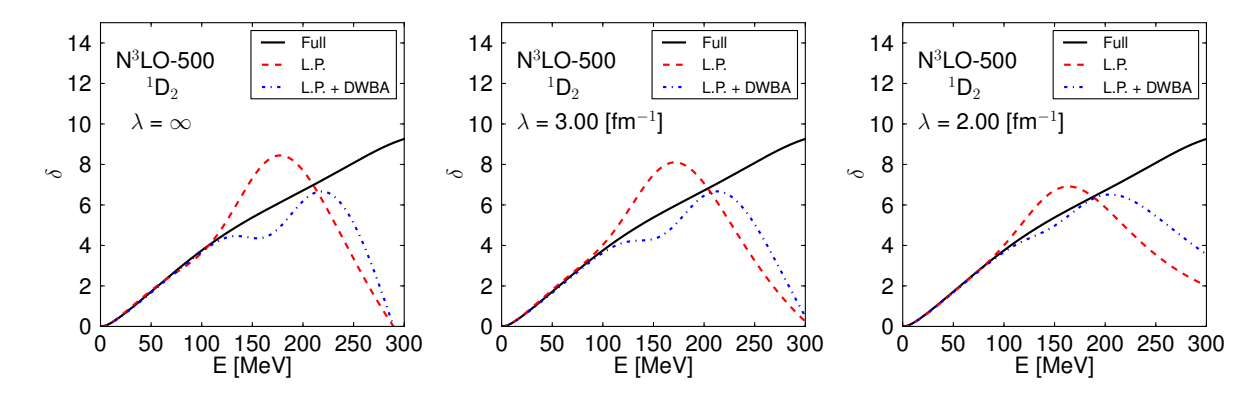


FIG. 10. (color online) Same as Fig. 9 except starting from Entem-Machleidt N³LO 500 MeV as the initial potential.

channel is non-trivial because of the fine tuning in the potential that generates the large S-wave scattering length. Above 100 MeV the phase shifts from the local potential are more attractive than the exact phase shifts, consistent with the removal of the hard core. The perturbative contribution increasingly overcorrects in this region. For the N³LO potential, the effect of evolving in λ is much less pronounced and the final results for $\lambda = 2 \, \mathrm{fm}^{-1}$ and below are very similar to Argonne v_{18} , as expected from the flow to a universal form in this channel.

The story for the $^1\mathrm{D}_2$ channel in Figs. 9 and 10 is qualitatively the same, except that the agreement at the lowest energies (below 50 MeV) remains very good in all cases. The deviations at higher energies are more severe for the $\mathrm{N}^3\mathrm{LO}$ potential because of the non-local regulator.

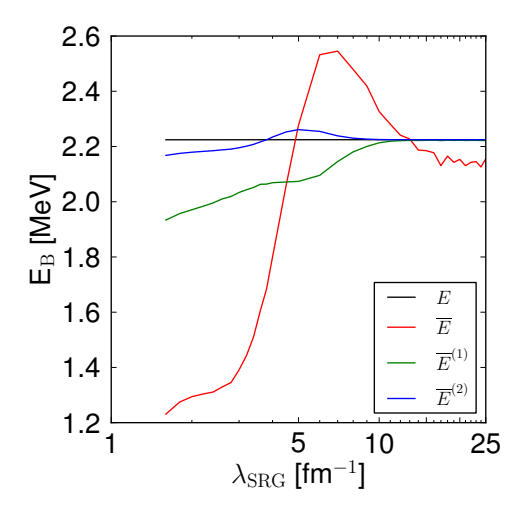


FIG. 11. (color online) Deuteron binding energy as a function of SRG λ , starting from the Argonne v_{18} potential. Exact results (E) are compared to the local projection (\overline{E}) and the first two orders of ordinary perturbation theory $(\overline{E}^{(1)})$ and $\overline{E}^{(2)}$.

In Figs. 11 and 12, we compare the deuteron binding energy from the full Argonne v_{18} and N³LO potentials,

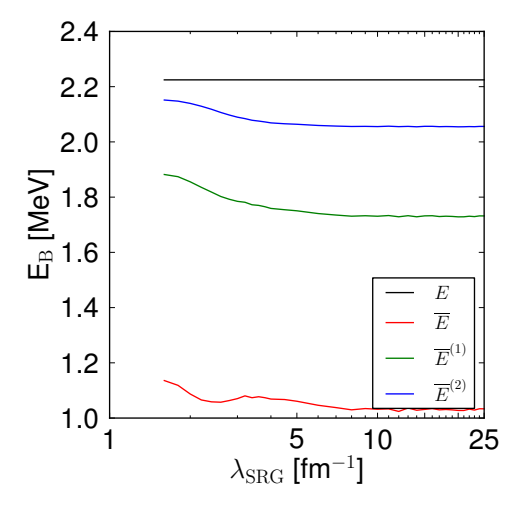


FIG. 12. (color online) Same as Fig. 11 except starting from the $\rm N^3LO~500\,MeV$ potential.

respectively, to the results from the local projection and the first two orders of perturbation theory. The deviations for the local projections are both significant, with similar results after evolution to λ below 3 fm⁻¹. The error reflects the fine-tuned cancellation between the kinetic energy and the potential energy; this fine-tuning is not as completely preserved by the local projection. Perturbation theory improves the energy at all λ values, with the second-order correction at $\lambda = 1.6 \, \mathrm{fm}^{-1}$ bringing the energy for both initial potentials within 100 keV.

We can also look at the probability densities for the deuteron, which are shown in Figs. 13 and 14, and the deuteron momentum distributions (i.e., the momentum-space wave function squared), which are shown in Figs. 15 and 16. While these are not observables, they can give insight into how the local projection modifies the nuclear wave functions. Short-range correlations for the initial potentials are associated with the "wound" at small r in coordinate space and the strong high-momentum components (e.g., for $k > 2 \, \mathrm{fm}^{-1}$) in momentum space. The SRG evolution fills in the wound and greatly suppresses the high-k strength. The deviations in the wave func-

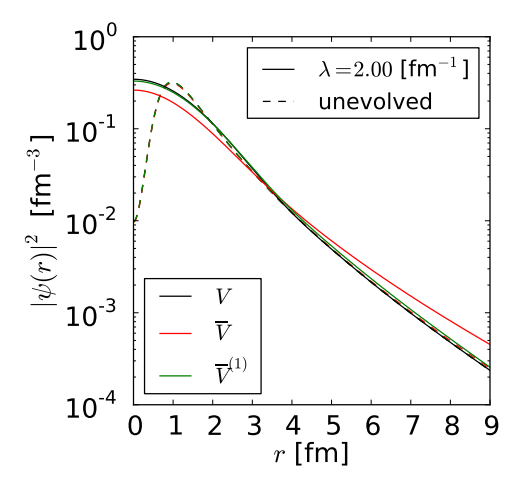


FIG. 13. (color online) The deuteron wave function squared calculated from the full interaction evolved to $\lambda = 2 \, \mathrm{fm}^{-1}$ starting from the Argonne v_{18} potential compared to the result using the local projection and first-order perturbation theory.

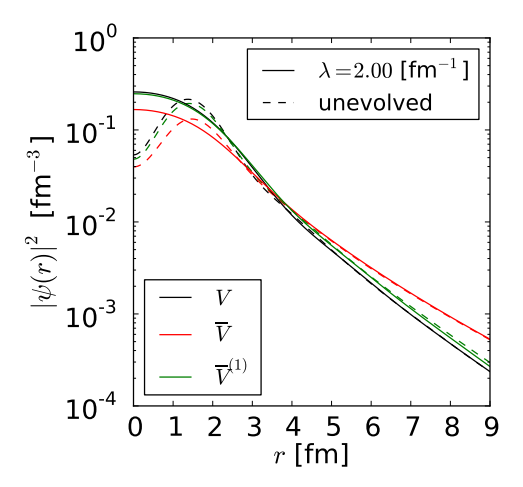


FIG. 14. (color online) Same as Fig. 15 except starting from the $\rm N^3LO~500\,MeV$ potential.

tions caused by the local projection are largely removed by first-order perturbation theory. The short-range correlations are also additionally suppressed by the local projection relative to the full evolved potential, but the qualitative interpretation is unchanged.

Finally, we can use Weinberg eigenvalues [34] as a diagnostic for changes in the NN potentials under local projection [35, 36]. In Fig. 17, we show the largest attractive and repulsive eigenvalues at zero energy for the $^{1}S_{0}$ channel as a representative example. The value of the large attractive eigenvalue, which approaches but is always less than one, reflects the near bound state in this channel. This is a physical property so we do not expect dramatic changes with decreasing λ . (Note: this eigenvalue would be equal to one for E=0 if there were a bound state precisely at zero energy.) The differences in eigenvalues

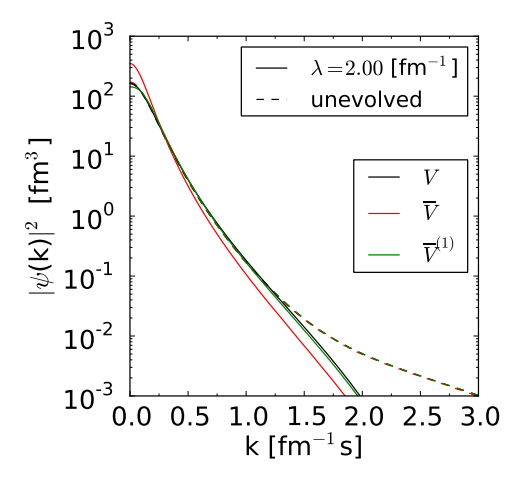


FIG. 15. (color online) The deuteron momentum distribution calculated from the full interaction evolved to $\lambda = 2 \, \mathrm{fm}^{-1}$ starting from the Argonne v_{18} potential compared to the result using the local projection and first-order perturbation theory.

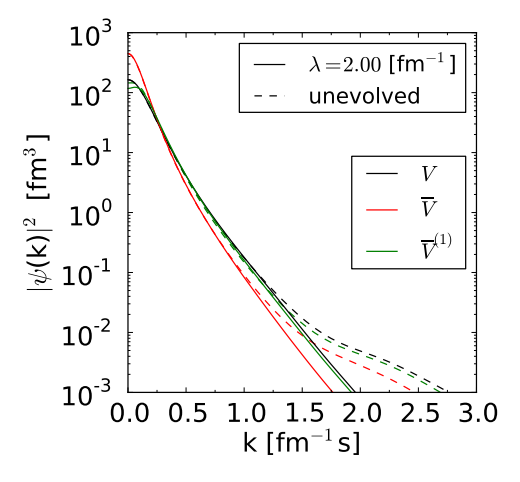


FIG. 16. (color online) Same as Fig. 15 except starting from the ${
m N}^3{
m LO}$ 500 MeV potential.

from the local projections and full potentials are consistent with the variations observed above for the deuteron energy. The extreme decrease of the largest repulsive eigenvalue for Argonne v_{18} quantifies the melting of the repulsive core as a result of SRG evolution. A significant but much smaller effect is seen for the N³LO potential, which is already comparatively soft initially. In both cases, the local projections generate eigenvalues that are always smaller than those from the full potential. This observation persists at all other energies. Thus the local projections are always at least as perturbative as the full potentials. The vanishing of the eigenvalues just below $\lambda = 4 \, \text{fm}^{-1}$ means that the negative of the potential fails to have a bound state [36]. This is consistent with the observed evolution of the potentials toward being purely attractive in this channel.

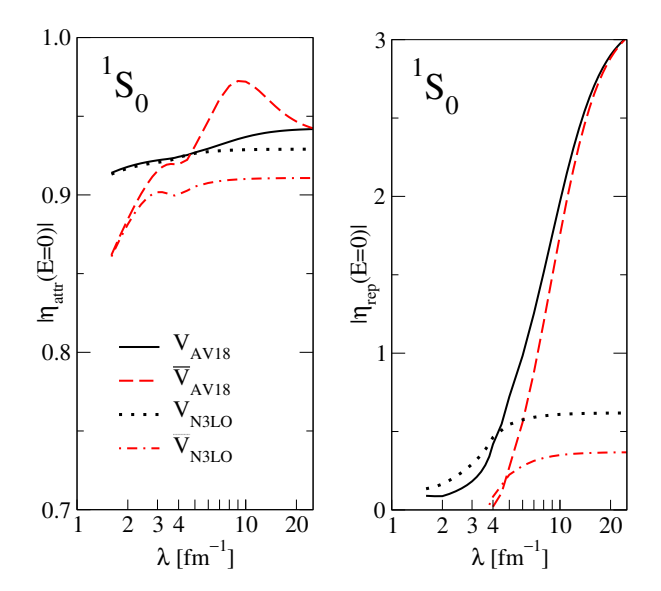


FIG. 17. (color online) Largest attractive and repulsive Weinberg eigenvalues at energy E=0 in the $^1\mathrm{S}_0$ channel as a function of SRG λ for Argonne v_{18} and N³LO initial potentials. The local projection \overline{V} is compared to the full evolved potential in each case.

V. SUMMARY

The renormalization group evolution of nucleonnucleon potentials to decouple low momenta from high momenta leads to increasingly non-local interactions. The non-localities inhibit clean visualizations in coordinate space and therefore make it difficult to develop an intuitive picture of the softening at different ranges. To overcome this limitation, we have studied a local projection (or non-local average) of the interaction. As we follow the flow of the projection, we can see directly that the repulsive core dissolves first, and only later in the evolution do longer-ranged features become modified. For the S-waves and some (but not all) other partial waves, the local projections from different initial potentials approach a common form at all ranges (which is purely attractive in the S-waves).

The observed pattern of non-locality agrees with conventional wisdom that the non-locality generated by RG evolution to lower resolution increases with the momentum transfer q [13]. For example, the dominant effect of evolution for off-diagonal matrix elements is the application of a non-local form factor:

$$V_{\lambda}(\mathbf{k}, \mathbf{k}') \stackrel{k \neq k'}{\approx} e^{-(\mathbf{k}^{2} - \mathbf{k}'^{2})^{2}/\lambda^{4}} V_{\lambda = \infty}(\mathbf{k}, \mathbf{k}')$$

$$= e^{-(\mathbf{k} + \mathbf{k}')^{2}/(\lambda^{4}/\mathbf{q}^{2})} V_{\lambda = \infty}(\mathbf{k}, \mathbf{k}') . \quad (26)$$

This contrasts with a Perey-Buck-type factorized non-

local potential [37] such as

$$V(\mathbf{r}, \mathbf{r}') = V_{\text{local}}[(\mathbf{r} + \mathbf{r}'/2)] \frac{1}{(\pi^{1/2}\beta)^3} e^{-(\mathbf{r} - \mathbf{r}')^2/\beta^2},$$
 (27)

for which the non-locality β is independent of the momentum transfer. The preservation of locality for low-momentum transfer is consistent with physical constraints that the longest-ranged part of the interaction is governed by pion exchange.

A local projection separates the full potential into a local piece and a purely non-local residual (this means that it is annihilated by a second projection). We find that low-energy observables calculated with the local projection of evolved interactions alone are reasonably well reproduced, with greater deviations for fine-tuned observables and at higher energies. Including corrections from the non-local residual potential in perturbation theory reduces deviations of phase shifts to the few percent level up to about 100 MeV (after which there remain significant deviations) and can correct the deuteron binding to better than 100 keV. This implies that the bulk of the low-energy physics is actually determined by local interactions and the purely non-local corrections are perturbative.

If the higher-energy contributions are sufficiently decoupled, our results suggest a possible strategy for applying low-momentum potentials in QMC calculations. Namely one can use existing technology with the local projection part of the interaction and then correct the result in perturbation theory. While the accuracy achieved in the test cases examined here may not be competitive with direct use of local potentials such as Argonne v_{18} , the particular choice of local projection considered has not been optimized in any way. Further tests including different choices for the projection are needed before judging the feasibility of this program. More importantly, one needs to include the contributions of many-body interactions, which is also of great current interest for visualizing the nature of induced three- and four-body forces effects during SRG evolution (including the effects of different choices of SRG generators). Work on this is in progress using a hyperspherical representation.

ACKNOWLEDGMENTS

We gratefully acknowledge A. Nogga for suggesting local projections as a visualization tool. We thank E. Anderson, S. Bogner, B. Dainton, K. Hebeler, H. Hergert, R. Perry, and A. Schwenk for useful comments and discussions. This work was supported in part by the National Science Foundation under Grant No. PHY–1002478, the UNEDF SciDAC Collaboration under DOE Grant DE-FC02-07ER41457, and by the DOE Office of Science Graduate Fellowship (SCGF) program under DOE contract number DE-AC05-06OR23100.

- [1] M. Preston and R. Bhaduri, Structure of the nucleus (Addison-Wesley, 1975).
- [2] K. Krane and D. Halliday, Introductory nuclear physics (Wiley, 1987).
- [3] B. Povh, K. Rith, C. Scholz, and F. Zetsche, *Particles and nuclei: an introduction to the physical concepts; 4th ed.* (Springer, Berlin, 2004).
- [4] E. Epelbaum, H.-W. Hammer, and U.-G. Meissner, Rev. Mod. Phys. 81, 1773 (2009).
- [5] H. Ekstein, Phys. Rev. 117, 1590 (1960).
- [6] L. Frankfurt, M. Sargsian, and M. Strikman, Int. J. Mod. Phys. A 23, 2991 (2008).
- [7] S. C. Pieper and R. B. Wiringa, Ann. Rev. Nucl. Part. Sci. 51, 53 (2001).
- [8] S. C. Pieper, Nucl. Phys. A **751**, 516 (2005).
- [9] S. Fantoni, S. Gandolfi, A. Y. Illarionov, K. E. Schmidt, and F. Pederiva, AIP Conf. Proc. 1056, 233 (2008).
- [10] R. B. Wiringa, V. G. J. Stoks, and R. Schiavilla, Phys. Rev. C 51, 38 (1995).
- [11] D. R. Entem and R. Machleidt, Phys. Rev. C 68, 041001 (2003).
- [12] E. Epelbaum, W. Glockle, and U.-G. Meissner, Nucl. Phys. A 747, 362 (2005).
- [13] S. K. Bogner, R. J. Furnstahl, and A. Schwenk, Prog. Part. Nucl. Phys. 65, 94 (2010).
- [14] R. Mehrem and A. Hohenegger, J.Phys.A A43, 455204 (2010).
- [15] S. D. Glazek and K. G. Wilson, Phys. Rev. D 48, 5863 (1993).
- [16] F. Wegner, Ann. Phys. (Berlin) **506**, 77 (1994).
- [17] S. Kehrein, The Flow Equation Approach to Many-Particle Systems (Springer, Berlin, 2006).
- [18] S. K. Bogner, R. J. Furnstahl, and R. J. Perry, Phys. Rev. C 75, 061001 (2007).

- [19] S. K. Bogner et al., Nucl. Phys. A 801, 21 (2008).
- [20] E. D. Jurgenson, P. Navratil, and R. J. Furnstahl, Phys. Rev. Lett. 103, 082501 (2009).
- [21] K. Hebeler, S. Bogner, R. Furnstahl, A. Nogga, and A. Schwenk, Phys. Rev. C 83, 031301 (2011).
- [22] P. Navratil, R. Roth, and S. Quaglioni, Phys. Rev. C 82, 034609 (2010).
- [23] P. Navratil, S. Quaglioni, and R. Roth, J.Phys.Conf.Ser. 312, 082002 (2011).
- [24] E. Jurgenson, P. Navratil, and R. Furnstahl, Phys. Rev. C ${\bf 83},\,034301$ (2011).
- [25] H. Hergert, P. Papakonstantinou, and R. Roth, Phys.Rev. C83, 064317 (2011).
- [26] R. Roth, S. Binder, K. Vobig, A. Calci, J. Langhammer, et al., nucl-th/1112.0287 (2011).
- [27] S. D. Glazek and R. J. Perry, Phys. Rev. D 78, 045011 (2008).
- [28] K. Wendt, R. Furnstahl, and R. Perry, Phys. Rev. C 83, 034005 (2011).
- [29] J. D. Holt, T. Kuo, G. Brown, and S. K. Bogner, Nuclear Physics A 733, 153 (2004).
- [30] S. K. Bogner, A. Schwenk, R. J. Furnstahl, and A. Nogga, Nucl. Phys. A 763, 59 (2005).
- [31] J. Taylor, Scattering Theory: The Quantum Theory of Nonrelativistic Collisions (Dover, 2006).
- [32] M. Bolsterli, Phys.Rev.Lett. **32**, 436 (1974).
- [33] R. Newton, Scattering theory of waves and particles (Dover, 2002).
- [34] S. Weinberg, Phys. Rev. **131**, 440 (1963).
- [35] S. K. Bogner, R. J. Furnstahl, S. Ramanan, and A. Schwenk, Nucl. Phys. A 773, 203 (2006).
- [36] S. Ramanan, S. K. Bogner, and R. J. Furnstahl, Nucl. Phys. A 797, 81 (2007).
- [37] F. G. Perey and B. Buck, Nucl. Phys. A 32, 353 (1962).